ADDITIONAL FILE 1

Gut microbiota contributes to high-altitude hypoxia acclimatization of human populations

Qian Su[1,5#], Dao-Hua Zhuang[2#], Yu-Chun Li[1#], Yu Chen[3#], Xia-Yan Wang[1#], Ming-Xia Ge[1], Ting-Yue Xue[1], Qi-Yuan Zhang[1], Xin-Yuan Liu[3], Fan-Qian Yin[1], Yi-Ming Han[1], Zong-Liang Gao[1], Long Zhao[1], Yong-Xuan Li[1], Meng-Jiao Lv[1], Li-Qin Yang[1], Tian-Rui Xia[1], Yong-Jun Luo[3*], Zhigang Zhang[2*], Qing-Peng Kong[1,4*]

[1]Key Laboratory of Genetic Evolution & Animal Models (Chinese Academy of Sciences), Key Laboratory of Healthy Aging Research of Yunnan Province, Kunming Key Laboratory of Healthy Aging Study, KIZ/CUHK Joint Laboratory of Bioresources and Molecular Research in Common Diseases, Kunming Institute of Zoology, Chinese Academy of Sciences, Kunming, Yunnan 650201, China;
[2]State Key Laboratory for Conservation and Utilization of Bio-Resources in Yunnan, School of Life Sciences, Yunnan University, Kunming, Yunnan 650091, China;
[3]Department of Military Medical Geography, Army Health Service Training Base, Third Military Medical University, Chongqing 400038, China;
[4]CAS Center for Excellence in Animal Evolution and Genetics, Chinese Academy of Sciences, Kunming 650223, China;
[5]University of Chinese Academy of Sciences, Beijing 100049, China.

[#]These authors contributed equally to this work.

[*]Correspondence: kongqp@mail.kiz.ac.cn (Q.-P.K.), zhangzhigang@ynu.edu.cn (Z.-G.Z.), luo.yongjun@qq.com (Y.-J.L.)

SUPPLEMENTARY FIGURES

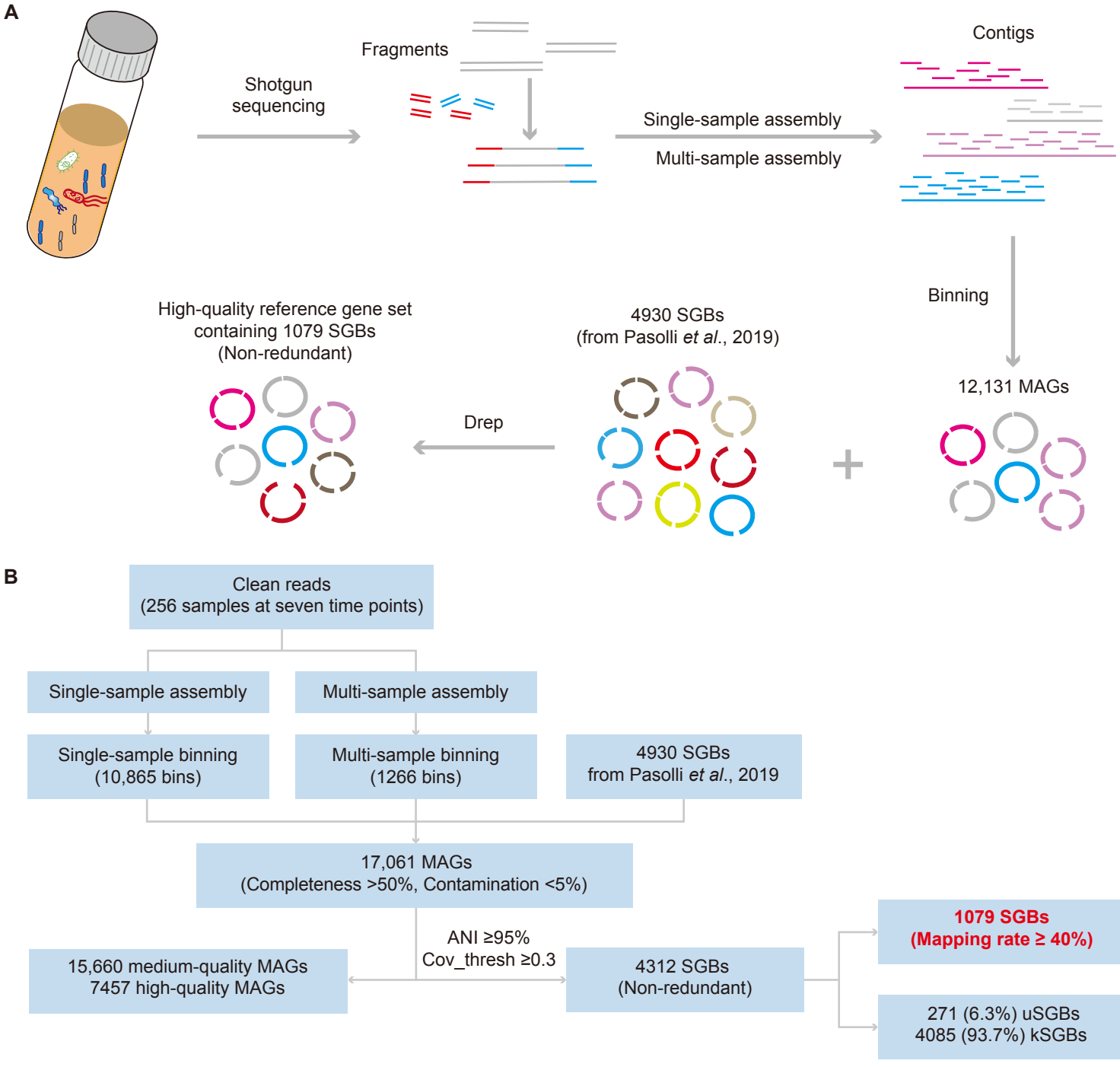

Figure S1. Pipeline for constructing a non-redundant genome set of the human gut microbiome under high-altitude exposure.

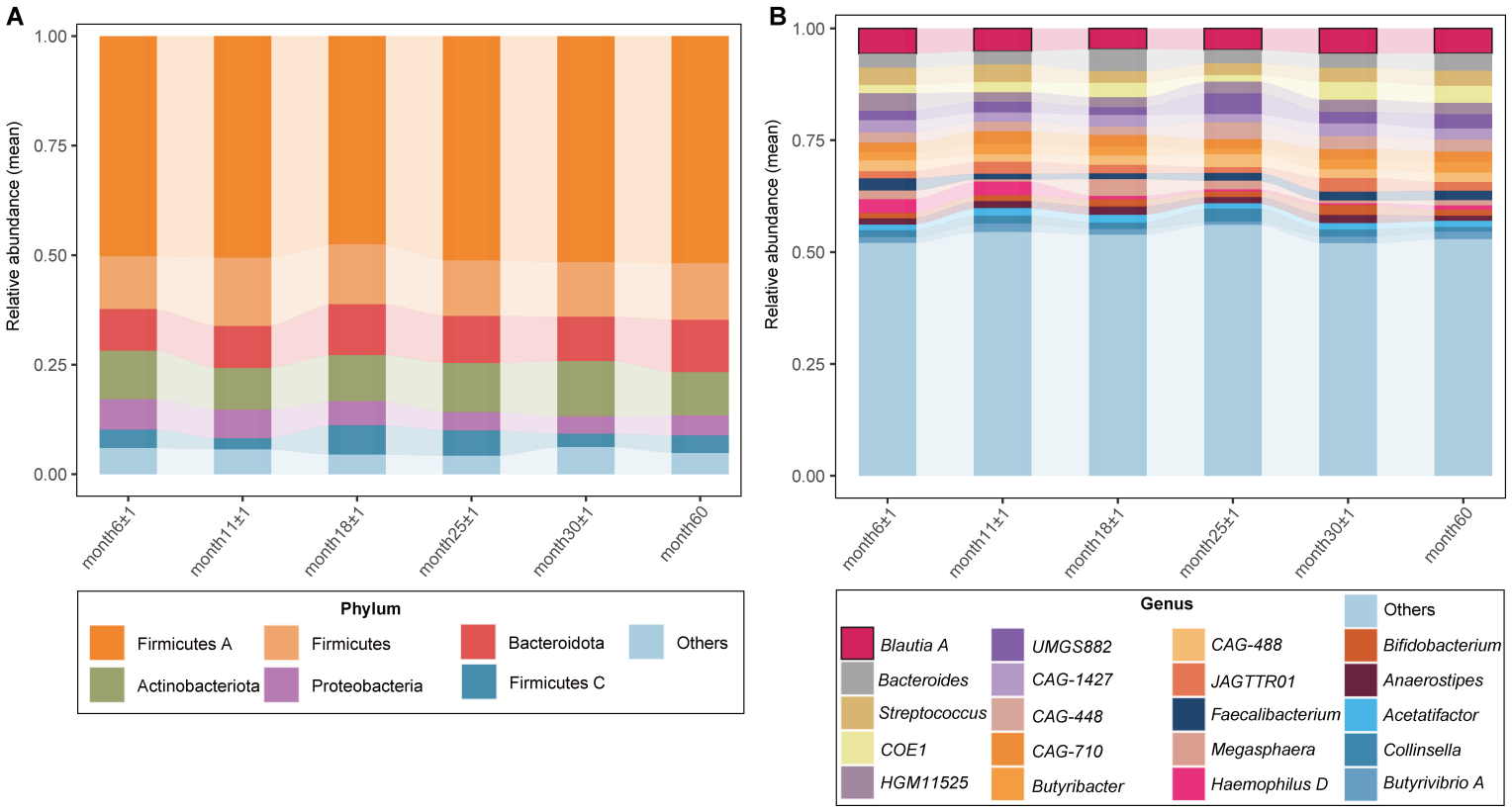

Figure S2. Temporal changes in gut microbiota composition across distinct taxa (phyla and genera) in six Shigatse, Xizang populations. Alluvial plot showing relative abundance dynamics in (A) six most abundant phyla and (B) 20 most abundant genera. Low-abundance taxa are grouped as "others". Ordinate represents mean relative abundance at each timepoint.

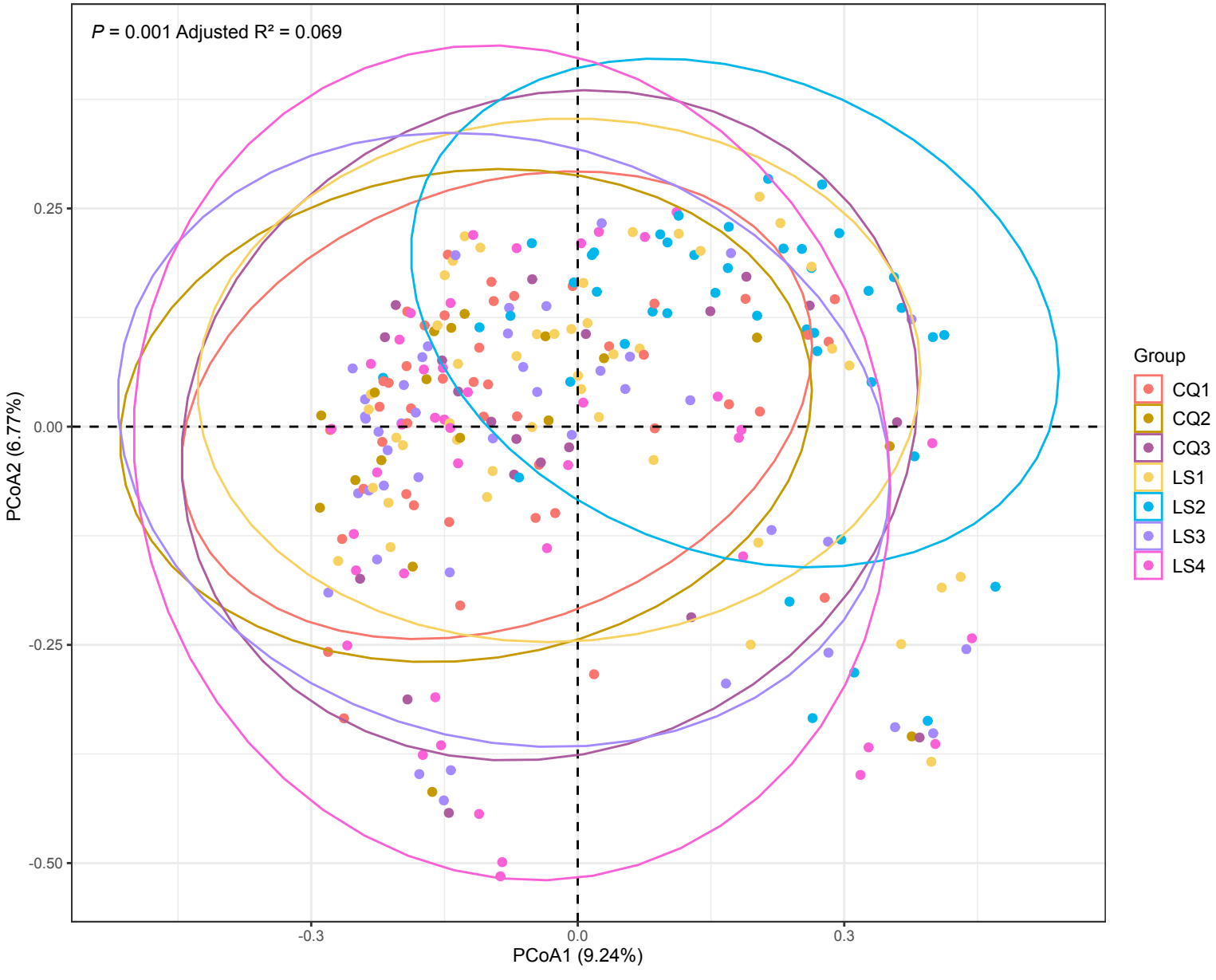

Figure S3. Principal coordinate analysis (PCoA) based on Bray-Curtis distances of SGB profiles. Different colors represent different timepoints. Dots represent different samples at seven timepoints. Permutation multiple analysis of variance (PERMANOVA) is used to determine significance. Adjusted R^2 explains the adjusted effect size.

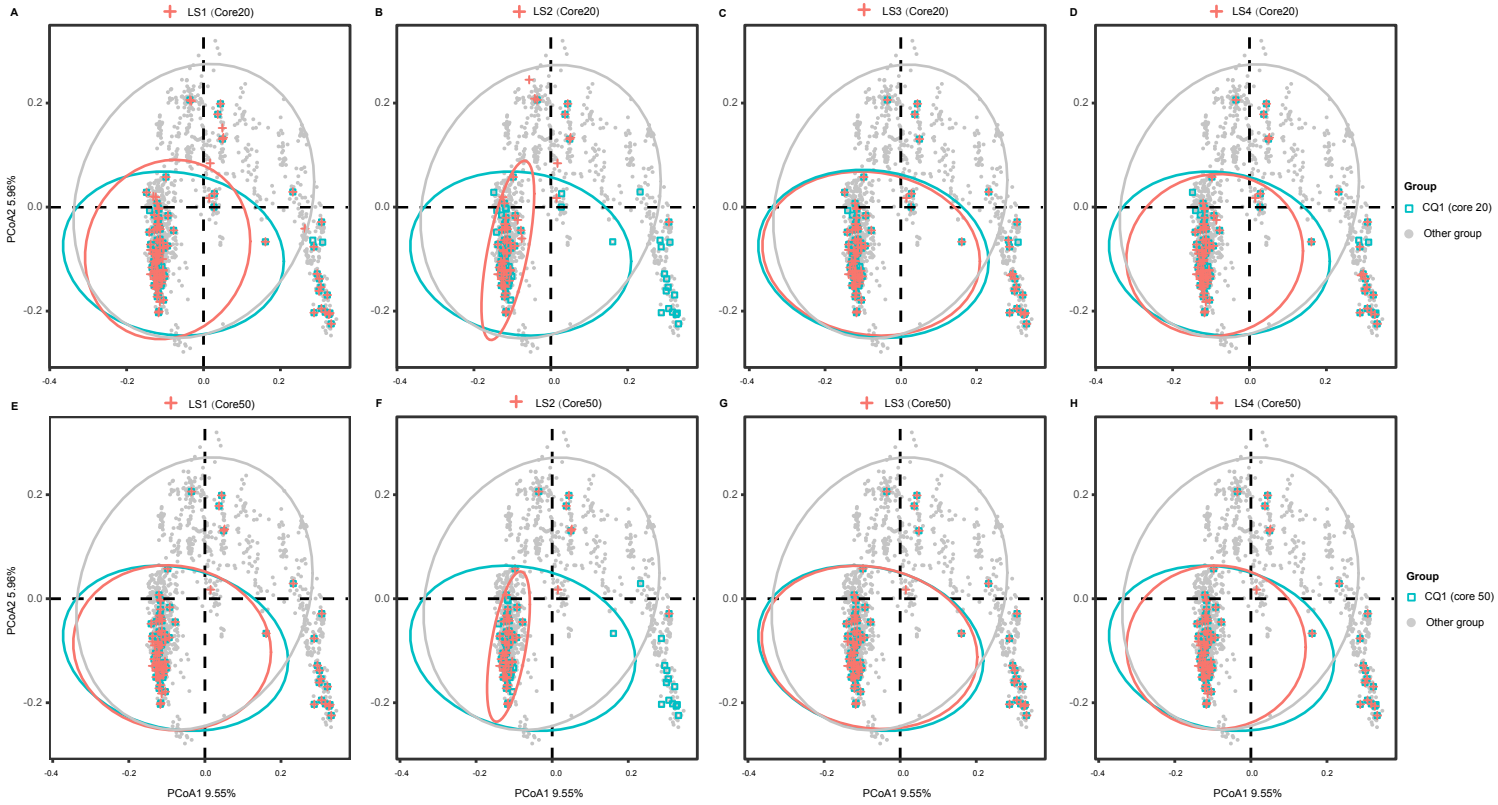

Figure S4. PCoA based on Bray-Curtis distance of SGB-KO (KEGG Orthology) matrix. Each dot represents an SGB. Gray dots represent all 1079 SGBs. Red dots represent core SGBs at corresponding exposure timepoint. Cyan dots represent core SGBs at baseline (CQ1). (A-D): SGBs present in at least 20% of the 256 samples (core 20); (E-H): SGBs present in at least 50% of the 256 samples (core 50).

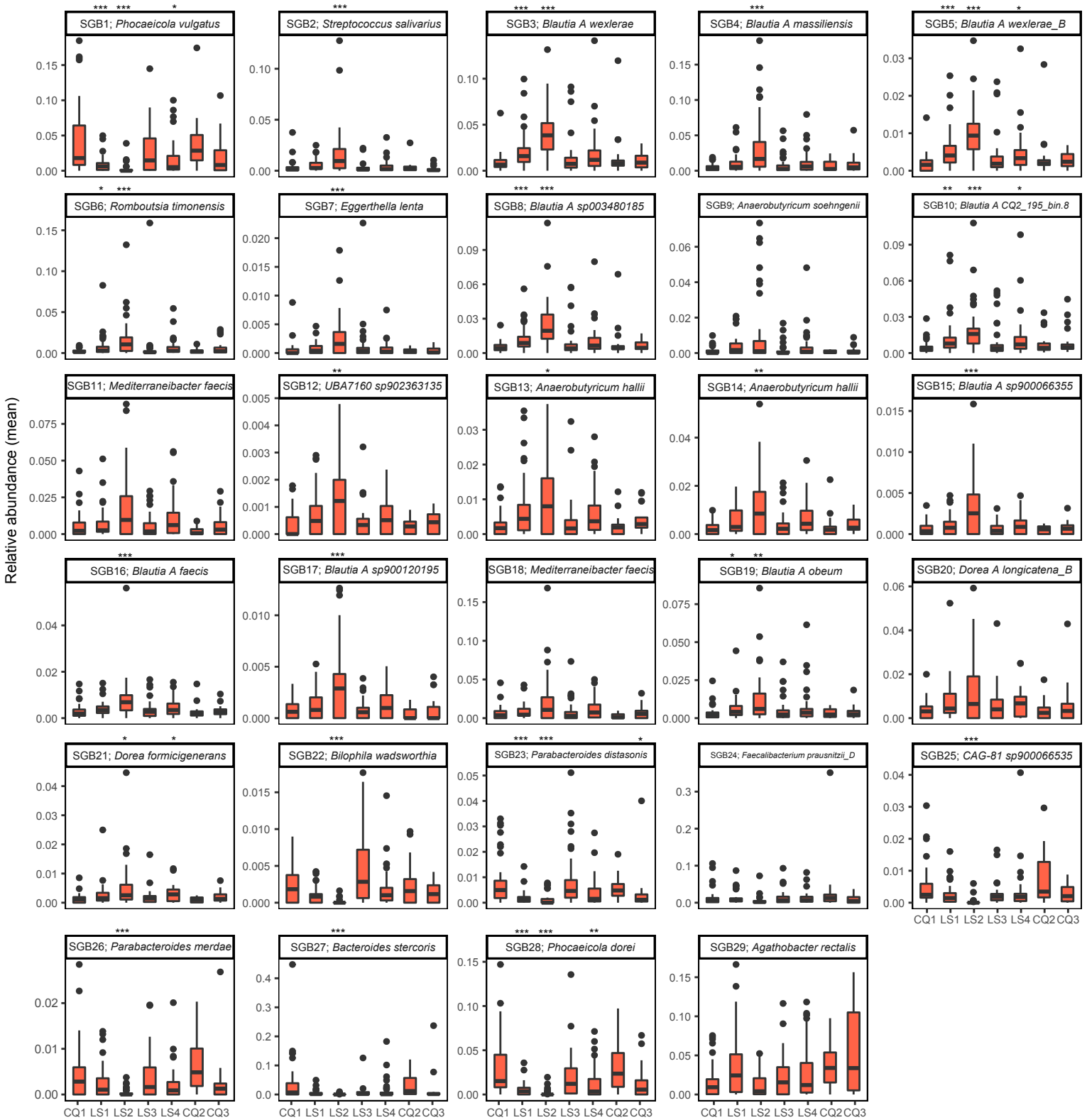

Figure S5. Relative abundance histograms of 29 indicator SGBs at different exposure stages. Paired Wilcoxon Rank Sum test is used to analyze differences between groups (*$P < 0.05$, **$P < 0.01$, ***$P < 0.001$). Ordinate reflects relative abundance of indicator SGBs.

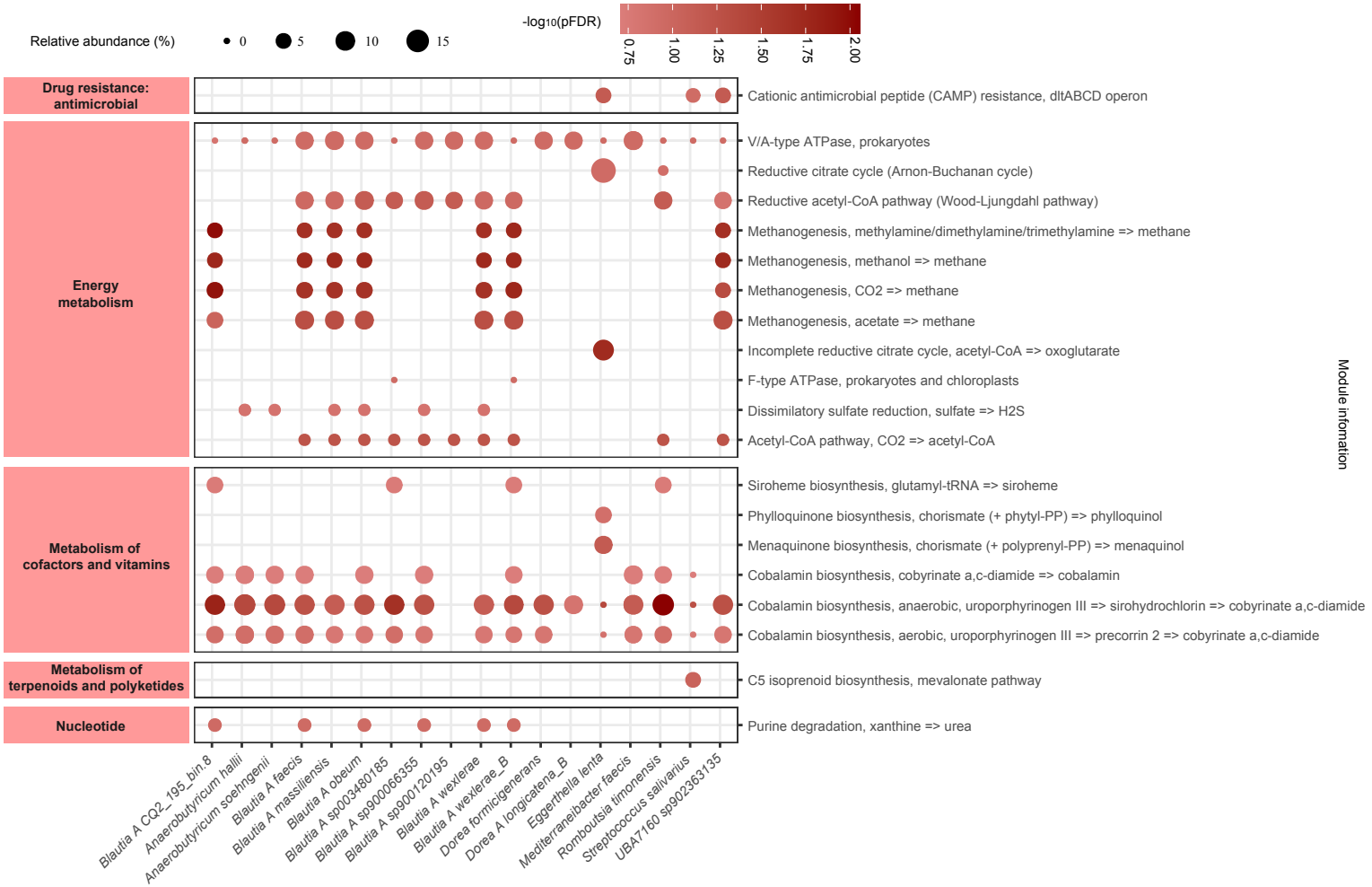

Figure S6. Point graph of functional module enrichment of single indicators. Left panel corresponds to KEGG metabolism category. Dot size represents the number of enriched genes in functional modules. Dot color gradient reflects the magnitude of -log10(pFDR).

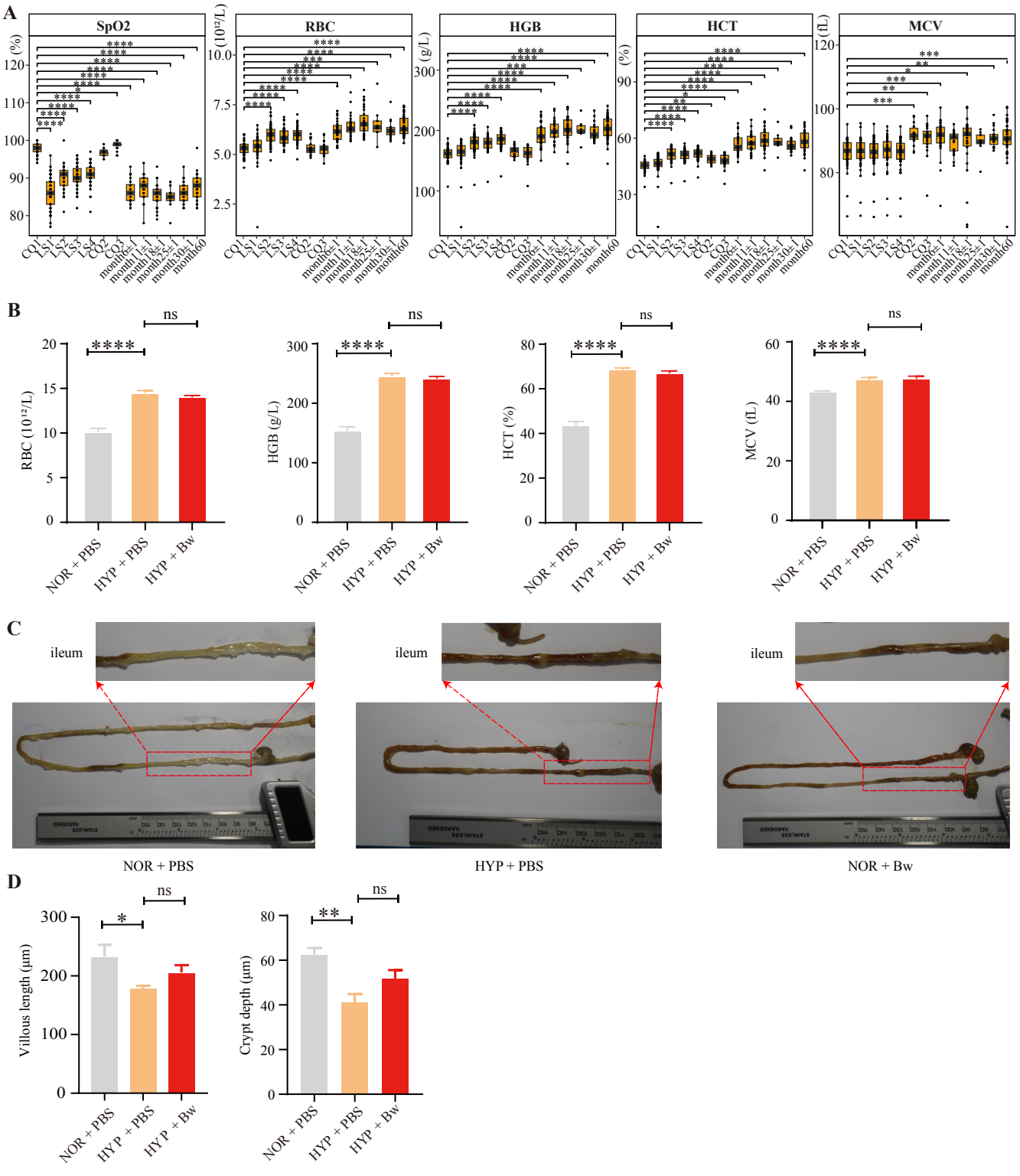

Figure S7. Hematologic parameters and intestinal morphology of mice at different exposure stages. (A) Dynamics of erythrocyte parameters during short-term and long-term high-altitude exposure. Values are mean ± SE. *$P < 0.05$, **$P < 0.01$, ***$P < 0.001$ (unpaired Wilcoxon Rank Sum test). (B) Erythrocyte parameters in NOR+PBS, HYP+PBS, and HYP+Bw mice after 8-week of intervene (n=8 per group). Values are mean ± SE. *$P < 0.05$; **$P < 0.01$; ***$P < 0.001$; ns, not significant (one-way ANOVA with Dunnett's multiple comparisons test). (C) Morphological appearance of the intestinal tract in NOR+PBS, HYP+PBS, and HYP+Bw mice after 8-week of intervention. (D) Statistical analysis of villus length and crypt depth in the distal ileum of mice (n=5 per group). Values are mean ± SE. *$P < 0.05$; **$P < 0.01$; ***$P < 0.001$; ns, not significant (one-way ANOVA with Dunnett's multiple comparisons test).

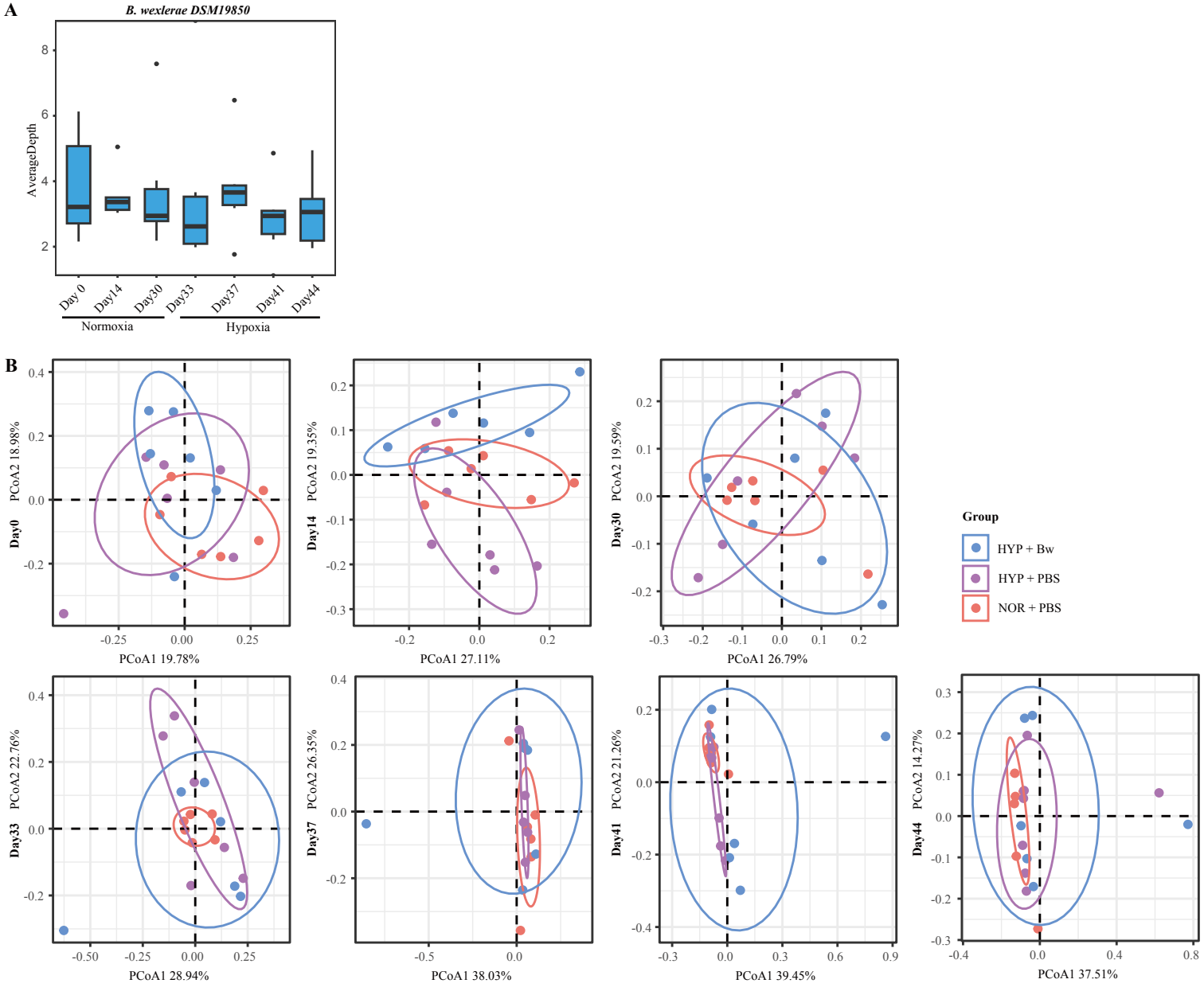

Figure S8. Taxonomic dendrogram of 4312 SGBs constructed using GraPhlAn based on Genome Taxonomy Database (GTDB) taxonomy information. Branch colors represent phylum classification. The three internal bands indicate known SGBs[1], newly identified SGBs from our study, and shared SGBs. The outer purple bar graph shows the number of MAGs clustered into SGBs.

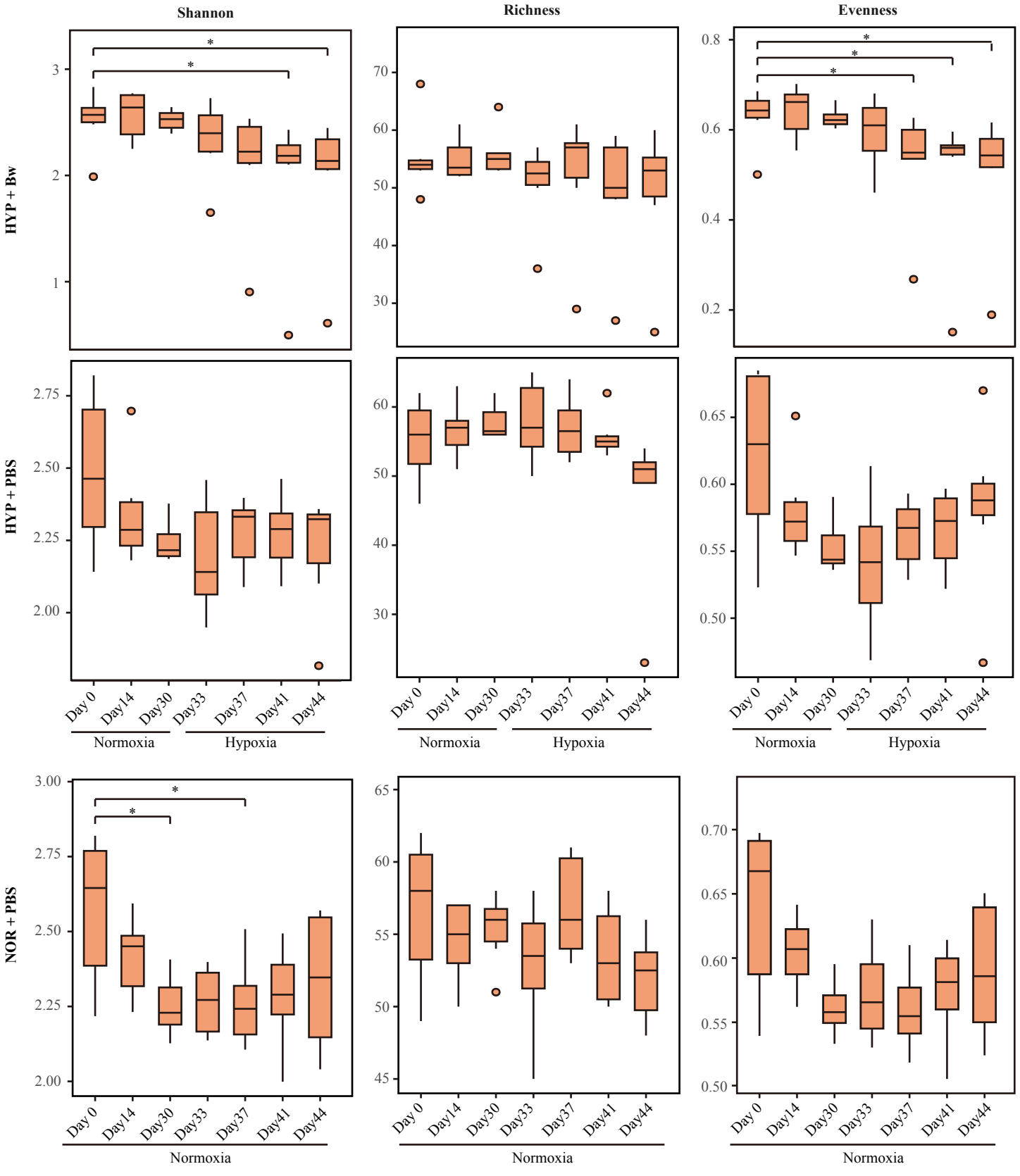

Figure S9. Dynamics of intestinal *B. wexlerae* colonization and PCoA graph in mice across different exposure timepoints. (A) Average depth of *B. wexlerae* DSM19850 (Bw) in each sample. (B) PCoA graph of gut microbiota in mice based on species-level Bray-Curtis distances. Three groups of mice (HYP+PBS, HYP+PBS, NOR+PBS) received oral gavage with Bw (1×10^9 CFU/ml) or PBS every 2 days, followed by analysis of fecal bacterial composition dynamics using metagenomic sequencing. Data represent seven distinct gavage timepoints (n = 6 per group).

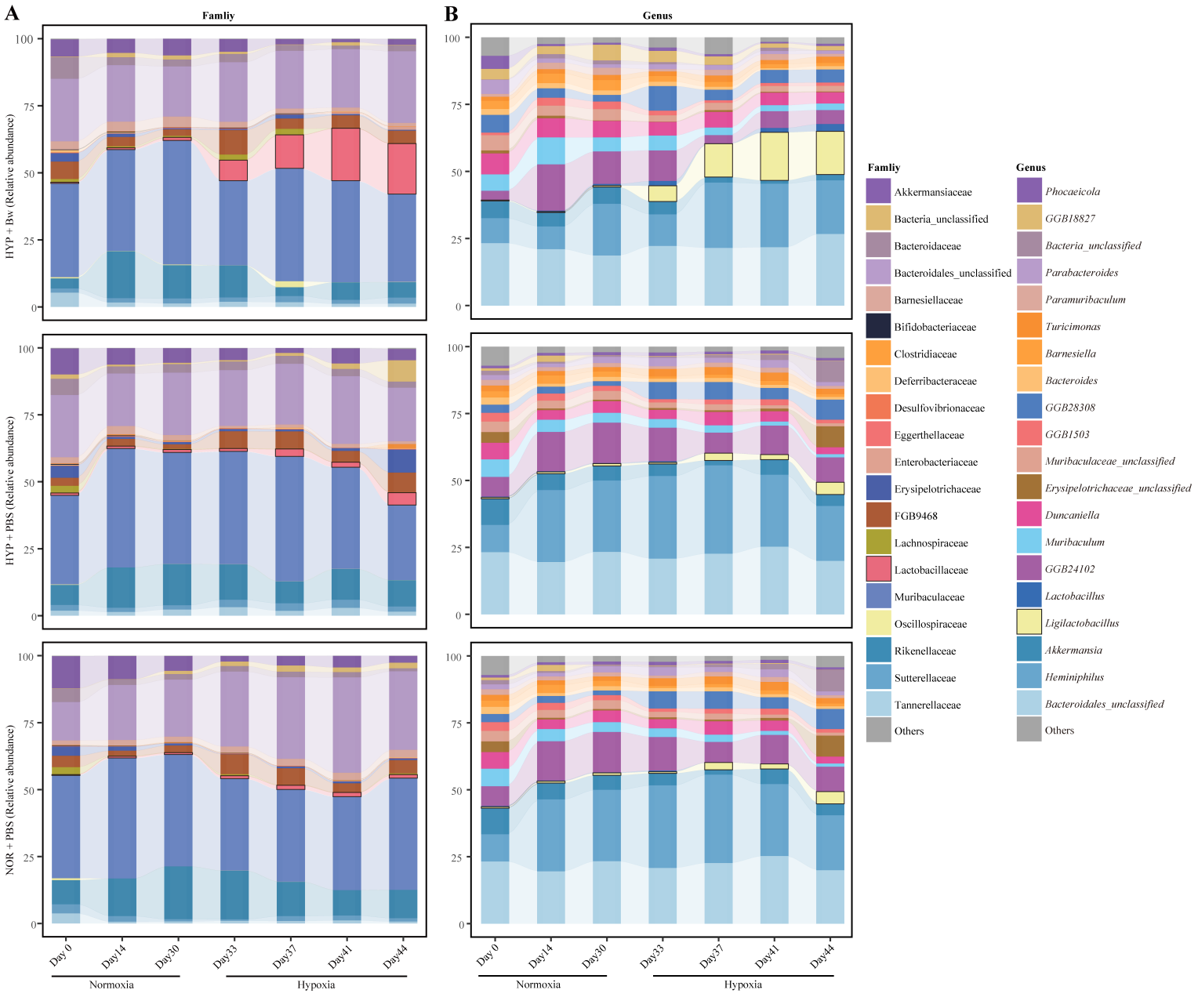

Figure S10. Dynamic changes in the alpha diversity of mouse gut microbiota. Boxplot of alpha diversity changes in three groups of mice (HYP+PBS, HYP+PBS, NOR+PBS), including Shannon, richness, and evenness indices. Data represent seven distinct gavage timepoints (n = 6 per group).

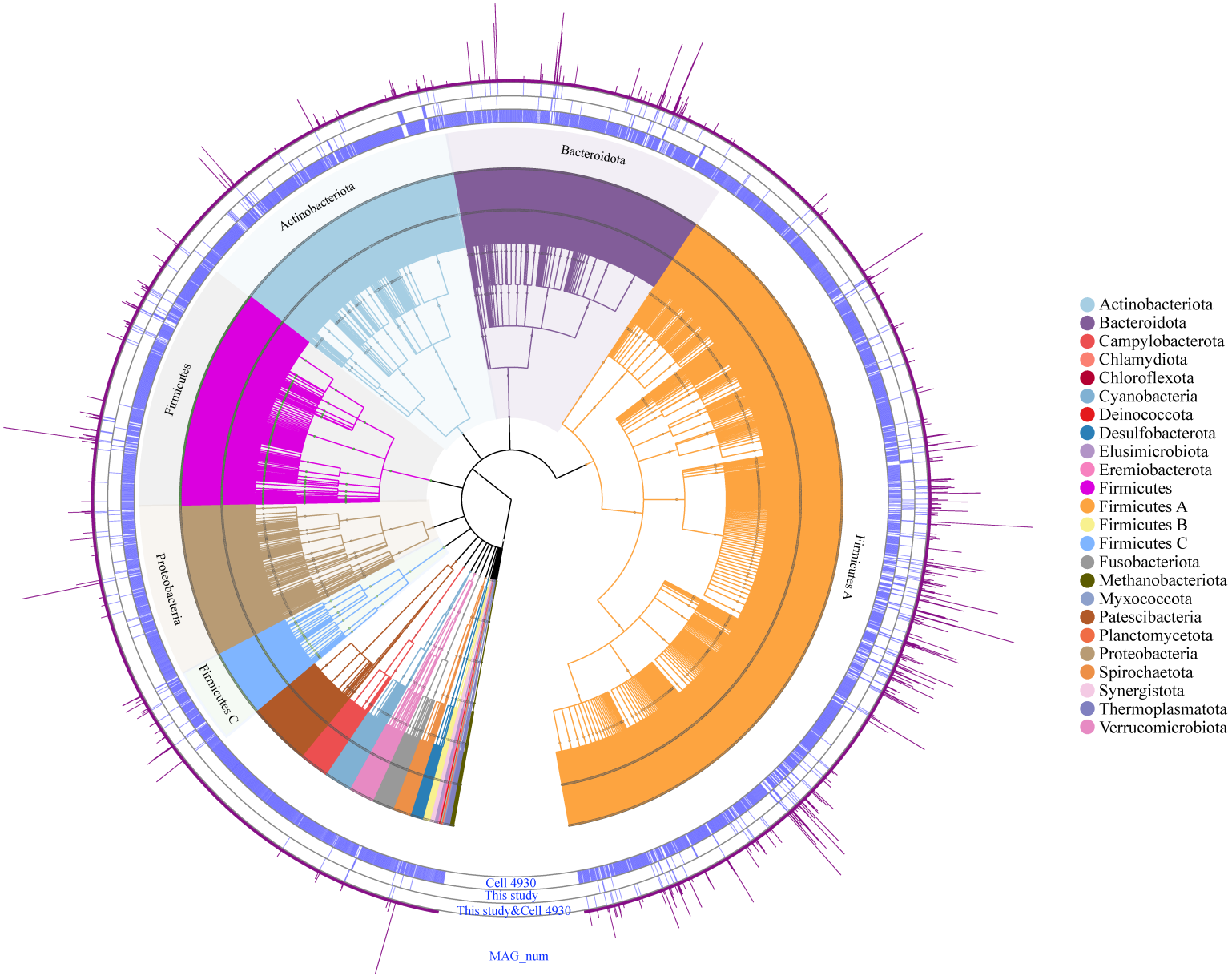

Figure S11. Dynamic changes in the community composition of mouse gut microbiota at the family and genus taxa. Alluvial plots illustrate the mean relative abundance dynamic of (A) seven most abundant families and (B) 20 most abundant genera across three mouse groups (HYP+PBS, HYP+PBS, NOR+PBS). Low-abundance taxa are grouped as “others.” Data represent seven distinct gavage timepoints (n = 6 per group).

References:

1. Pasolli E, Asnicar F, Manara S, Zolfo M, Karcher N, Armanini F, Beghini F, Manghi P, Tett A, Ghensi P, et al. Extensive unexplored human microbiome diversity revealed by over 150,000 genomes from metagenomes spanning age, geography, and lifestyle. Cell. 2019;176:649-62.